Journal of Power Sources 376 (2018) 100–110

Contents lists available at ScienceDirect

Journal of Power Sources

journal homepage: www.elsevier.com/locate/jpowsour

Mitigation of chromium poisoning of cathodes in solid oxide fuel cells employing $CuMn_{1.8}O_4$ spinel coating on metallic interconnect

Ruofan Wang[a,1], Zhihao Sun[a], Uday B. Pal[a,b,*], Srikanth Gopalan[a,b], Soumendra N. Basu[a,b]

[a] Division of Materials Science and Engineering, Boston University, Brookline, MA 02446, USA
[b] Department of Mechanical Engineering, Boston University, Boston, MA 02215, USA

HIGHLIGHTS

- Performances of dense and porous Cu-Mn spinel coatings were compared in cell tests.
- Cr-poisoning occurs in open-circuit condition as well as under resistive load.
- Cr species diffuse into cathode via both gaseous and solid-state pathways.
- Porous Cu-Mn coating shows limited Cr gettering capacity and lifetime.
- Dense Cu-Mn coating shows distinct improvement in mitigating Cr-poisoning effects.

ARTICLE INFO

Keywords:
Solid oxide fuel cells
Cathode
Chromium poisoning
Copper manganese spinel coatings
Interconnects
Degradation

ABSTRACT

Chromium poisoning is one of the major reasons for cathode performance degradation in solid oxide fuel cells (SOFCs). To mitigate the effect of Cr-poisoning, a protective coating on the surface of interconnect for suppressing Cr vaporization is necessary. Among the various coating materials, Cu-Mn spinel coating is considered to be a potential candidate due to their good thermal compatibility, high stability and good electronic conductivity at high temperature. In this study, Crofer 22 H meshes with no protective coating, those with commercial $CuMn_2O_4$ spinel coating and the ones with lab-developed $CuMn_{1.8}O_4$ spinel coating were investigated. The lab-developed $CuMn_{1.8}O_4$ spinel coating were deposited on Crofer 22 H mesh by electrophoretic deposition and densified by a reduction and re-oxidation process. With these different Crofer 22 H meshes (bare, $CuMn_2O_4$-coated, and $CuMn_{1.8}O_4$-coated), anode-supported SOFCs with Sr-doped $LaMnO_3$-based cathode were electrochemically tested at 800 °C for total durations of up to 288 h. Comparing the mitigating effects of the two types of Cu-Mn spinel coatings on Cr-poisoning, it was found that the performance of the denser lab-developed $CuMn_{1.8}O_4$ spinel coating was distinctly better, showing no degradation in the cell electrochemical performance and significantly less Cr deposition near the cathode/electrolyte interface after the test.

1. Introduction

Lowering the operating temperature of solid oxide fuel cells to the intermediate range of 650–800 °C can not only improve the reliability and stability of SOFCs, but also enable the use of metallic alloys in interconnects and balance-of-plant (BoP) materials [1–5]. Compared with ceramic interconnects, metallic interconnects have higher electronic conductivity, higher thermal conductivity, better machinability and lower cost [1,4,6–8]. The most widely developed and studied metallic interconnect materials are the chromia-forming alloys due to their high thermal compatibility with other SOFC components, high oxidation resistance at high temperature, and the conductive chromium (Cr) containing oxide scale that forms on the alloy surface [3,4,7,8]. However, on the cathode side (oxidation environment), Cr-containing oxide scale can react with oxygen/moisture and form higher valent Cr-containing vapor species (e.g. CrO_3 and $CrO_2(OH)_2$) [9–13]. These Cr-containing vapor species can transport and deposit in the cathode and deteriorate its performance [1,2,14–24]. This degradation phenomenon, namely 'Cr-poisoning', is one of the major reasons for the performance degradation in the SOFC stacks.

To mitigate the Cr-poisoning effect, decreasing the amount of Cr-containing vapor species over interconnect becomes an obvious solution. Fe-Cr-Mn alloys such as Crofer 22 APU [25] and Crofer 22 H [26] (ThyssenKrupp VDM), Sanergy HT (Sandvik Materials Technology)

* Corresponding author. Division of Materials Science and Engineering, Boston University, Brookline, MA 02446, USA.
E-mail address: upal@bu.edu (U.B. Pal).
[1] Present address: Energy Conversion Group, Energy Technologies Area, Lawrence Berkeley National Laboratory, Berkeley, CA 94720, USA.

https://doi.org/10.1016/j.jpowsour.2017.11.069
Received 2 October 2017; Received in revised form 21 November 2017; Accepted 22 November 2017
Available online 28 November 2017
0378-7753/

[27] and ZMG 232 (Hitachi Metals) [28] have been widely developed for SOFC interconnect application. Due to the small amounts (0.3–0.5 wt%) of Manganese in the Fe-Cr alloys, these steels develop a well adherent $(Cr,Mn)_3O_4$ spinel top layer above the Cr_2O_3 layer at 800 and 850 °C, and Cr evaporation rate over them is 2–3 times slower than that over alloys with pure Cr_2O_3 scales such as Ducrolloy (Plansee), or with a noncontinuous $(Cr,Mn)_3O_4$ top layer such as E-brite (ATI Allegheny Ludlum) [29–32].

Although $(Cr,Mn)_3O_4$ top layer formed over the Fe-Cr-Mn alloys can effectively decrease the Cr evaporation rate, it has been shown that performance degradation caused by Cr-poisoning is still considerable when using these alloys as interconnect materials [13,20,21,23,33]. Thus, in order to mitigate the stack performance degradation, long-term stable protective coatings over the interconnect for minimizing the Cr vaporization are indispensable. Over the past 10 years, extensive efforts were made in the development of protective coatings for metallic interconnects [7,8]. Among various coating materials, composite spinel oxides appear to be the most promising candidate, due to their high conductivities and good capabilities in retarding oxidation of metallic interconnect and suppressing vaporization of chromium [8]. While $(Mn,Co)_3O_4$ spinels are the most studied to date [33–40], Cu-Mn spinels that have higher electronic conductivities and lower cost are recently receiving more attention [41–47].

In this paper, mitigation of Cr-poisoning employing a candidate $CuMn_{1.8}O_4$ spinel interconnect coating is demonstrated. $CuMn_{1.8}O_4$ spinel coating is deposited on Crofer 22 H mesh by electrophoretic deposition (EPD) and densified by a reduction and re-oxidation process. To evaluate the performance of the $CuMn_{1.8}O_4$ spinel coating, the spinel-coated Crofer 22 H mesh is employed in the electrochemical testing of anode-supported cell (ASC). To simulate the interconnect in the stack, the mesh is placed in direct contact with the SOFC cathode. For comparison, Crofer 22 H mesh with no protective coating and that with commercial $CuMn_2O_4$ spinel coating are also investigated. In addition to the electrochemical tests, microstructures of the different Crofer 22 H meshes and the corresponding cell cathodes are characterized and compared. The performances of two types of Cu-Mn spinel interconnect coatings, $CuMn_2O_4$ (commercial) and $CuMn_{1.8}O_4$ (lab-developed), in mitigating Cr-poisoning are evaluated, and the effect of coating density on degradation phenomena are discussed.

2. Experimental

2.1. Electrophoretic deposition (EPD) of $CuMn_{1.8}O_4$ spinel coating

A commerical ferritic stainless steel, Crofer 22 H with composition of 22.93 wt% Cr, 1.94 wt% W, 0.51 wt% Nb, 0.43 wt% Mn, 0.21 wt% Si, 0.07 wt% Ti, 0.02 wt% Al, 0.08 wt% La, 0.10 wt% Si, 0.07 wt% C, 0.015 wt% N and the balance in Fe, was used as the interconnect material in this study [26]. Crofer 22 H meshes with no coating and those with $CuMn_2O_4$ spinel coating were commercially available from Fiaxell SOFC Technologies (Switzerland) [48]. According to technical specifications, the $CuMn_2O_4$ coated mesh was sintered in air at 850 °C for 3 h. The meshes have opening of about 0.6 × 0.9 mm and thickness of 0.2 mm.

The uncoated Crofer 22 H meshes were used as the substrates for deposition of the $CuMn_{1.8}O_4$ spinel coating by the electrophoretic deposition (EPD) process in our laboratory (the substrates were ultrasonically cleaned in the mixture of acetone and ethanol prior to coating deposition). Powders of $CuMn_{1.8}O_4$ used for coating were synthesized by the glycine nitrate process (GNP). Propotional amounts of manganese nitrate ($Mn(NO_3)_2{\cdot}4H_2O$, Alfa Aesar, USA), copper nitrate ($Cu(NO_3)_2{\cdot}2.5H_2O$, Alfa Aesar, USA) and glycine (CH_2NH_2COOH, Alfa Aesar, USA) were dissolved in deionized water, stirred for 10 min, and heated on a hot plate at 100 °C for 25 min for evaporating the excess water. The temperature of the precursor was then raised until the autocombustion occurred. After the combustion reaction was completed, the powders were calcined at 800 °C for 2 h to remove any unreacted reactants.

The synthesized spinel powders were ball-milled in ethanol for 4 h with 0.3 mm zirconia balls (Tosoh. Corp, Japan) to reduce the particle size. The $CuMn_{1.8}O_4$ powders were then mixed with desired amounts of acetone, ethanol and iodine, and the mixture was used as suspension media for the EPD. The EPD was performed for 10 min at a constant voltage of 20 V. Due to the irregular shape of the meshes, instead of conventional uniaxial compaction, the as-deposited coating was densified by subjecting the samples to a thermal treatment process: reduction at 1000 °C for 24 h in forming gas (2% H_2 + 98% Ar) and then annealing in air at 850 °C for 100 h.

2.2. SOFC fabrication

The cells used in this study were comprised of 5 layers: a Ni/8YSZ (8 mol% Y_2O_3–92 mol% ZrO_2) anode substrate, a Ni/8YSZ anode interlayer, an 8YSZ electrolyte, a LSM (Sr-doped $LaMnO_3$)/8YSZ composite cathode active layer, and a LSM current collector layer. As-sintered cell structures consisting of two anode layers and electrolyte were commercially purchased (Materials and Systems Research Inc., USA). Cathode active layer and cathode current collector layer were screen printed over the electrolyte. Slurry for the composite cathode active layer were prepared by mixing $(La_{0.8}Sr_{0.2})_{0.95}MnO_{3-\delta}$ (Fuel Cell Materials, USA) and 8YSZ (Tosoh Corp., Japan) powders in a 1:1 wt ratio and ball milling the mixture for 10 h in alpha-terpineol (Alfa Aesar, USA) with the desired amount of pore former (Carbon lampblack, Fisher Scientific, USA) and binder (V6, Heraeus, USA). For preparation of slurry for the cathode current collector layer, LSM powders were ball milled for 24 h in alpha-terpineol with desired amount of pore former (Carbon black, Fisher Scientific, USA) and binder (V6, Heraeus, USA). After screen printing of each cathode layer, the structure was sintered at 1200 °C for 2 h. After the fabrication was completed, the thickness of cathode active layer and the cathode current collector layer were approximately 30 μm and 50 μm, respectively and the active cathode area was 2 cm^2.

2.3. On-cell tests employing interconnect meshes

On identical cells, Crofer 22 H meshes (a) with no protective coating, (b) with commercial $CuMn_2O_4$ coating, and (c) with lab-developed $CuMn_{1.8}O_4$ coating, were used individually as current collectors on the cathode side for electrochemical cell testing. Prior to the cell assembly, the Crofer 22 H mesh (bare/$CuMn_2O_4$ coated/$CuMn_{1.8}O_4$ coated) was cut into round pieces having the same area as the SOFC cathode (~2 cm^2), and was attached on the cathode with a LSM paste. A nickel mesh was also pre-attached on the anode with nickel paste (Fuel Cell Materials, USA). Fig. 1 shows the schematic of the cell structure and interconnect mesh during the cell testing. In the fixture for cell testing, a single cell was sandwiched between two alumina tubes. A gold gasket on the cathode side and a mica gasket on the anode side were used for sealing purpose. In addition, glass paste (Fuel Cell Store, USA) was applied outside the tube circumference to ensure gas tightness. Two silver wires on the cathode side and two nickel rods on the anode side were firmly pressed on the Crofer 22 H mesh and nickel mesh respectively, to ensure good contacts. On each side, one wire/rod was used for current application, and the other for voltage measurement. More details of the cell testing fixture have been previously published [23].

The cells were electrochemically tested at 800 °C. On the anode side, humidified hydrogen with 2% H_2O (obtained by passing hydrogen through a water bubbler at ~ 18 °C) was circulated at 300 cm^3/min, providing fuel under flooded condition and low fuel utilization. On the cathode side, dry air was used over at 1000 cm^3/min (with gas velocity of approximately 4.8 m/s at 800 °C), which also provided a flooded condition with negligible fractional oxidant utilization. The cell testing

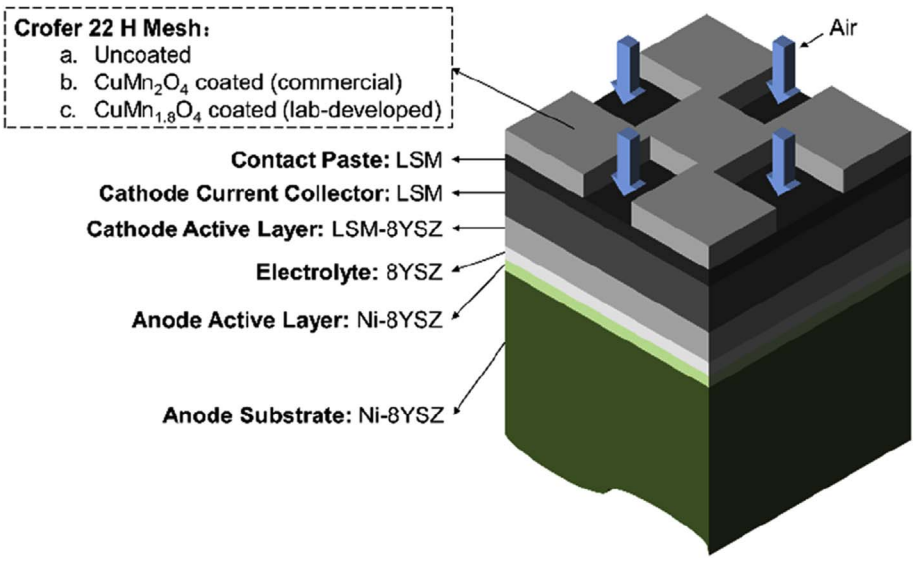

Fig. 1. A schematic of the cell structure and the interconnect mesh during cell testing.

procedure was as follows:

a. After the open-circuit voltage (OCV) of the cell was stable, current-voltage (C-V) measurement and electrochemical impedance spectroscopy (EIS, under open-circuit condition) were performed to characterize the initial cell performance (at t = 0 h).
b. The cell was then operated under open-circuit condition for 48 h. After that, the C-V and EIS measurements were carried out (at t = 48 h) to characterize the cell performance.
c. Cell was then operated under galvanostatic condition at 0.5 A/cm^2 (relative to the cathode area) for up to 240 h. The galvanostatic condition was interrupted by C-V and EIS measurements every 24 h to monitor the cell performance on a daily basis.

The details of the cell test conditions with uncoated, $CuMn_2O_4$ coated, and $CuMn_{1.8}O_4$ coated interconnect meshes, are summarized in Table 1. All electrochemical measurements were made with a Princeton Applied Research PARSTAT® 2273 potentiostat, and a KEPCO 20-20 M power amplifier.

2.4. Microstructural characterization

The surfaces of $CuMn_2O_4$ coating and $CuMn_{1.8}O_4$ spinel coating (after thermal treatments but before on-cell tests) were characterized by X-ray diffraction (XRD, Bruker D8 Advanced XRD system with CuKα radiation). The meshes with both $CuMn_2O_4$ and $CuMn_{1.8}O_4$ spinel coatings before and after the on-cell tests were sectioned and impregnated with epoxy. After the epoxy hardened, they were polished down to 0.05 μm and sputter-coated with carbon. The cross sections of the coatings were examined by scanning electron microscopy (SEM, Zeiss Supra 55VP) and energy dispersive X-ray spectroscopy (EDX, EDAX). After the electrochemical testing, the cells were fractured. The fractured cells were examined using the following methods:

a. To characterize the Cr intensity profile within the cathode on a flat cross section, one piece of each fractured cell was mounted (in epoxy), polished, sputter-coated (with carbon), and examined by SEM and EDX.
b. To observe the cathode/electrolyte interfaces with higher lateral resolution and contrast, another piece of each fractured cell (without epoxy mounting) was sputter-coated and examined by an in-lens detector (instead of conventional secondary-ion detector) in SEM. Elemental analysis of Cr-containing deposits near the cathode/electrolyte interfaces were performed by EDX.

Table 1
Cell test conditions with uncoated, $CuMn_2O_4$ coated, $CuMn_{1.8}O_4$ coated interconnect meshes.

Cell	Interconnect coating	Current condition	Total duration
Cell 1	No coating	48 h of open-circuit + 144 h of close-circuit at 0.5 A/cm^2	192 h
Cell 2	$CuMn_2O_4$ coating	48 h of open-circuit + 240 h of close-circuit at 0.5 A/cm^2	288 h
Cell 3	$CuMn_{1.8}O_4$ coating	48 h of open-circuit + 240 h of close-circuit at 0.5 A/cm^2	288 h

3. Results and discussion

3.1. Characterizations of coatings before on-cell testing

Fig. 2a and b show the cross-sections of commercial $CuMn_2O_4$ and lab-developed $CuMn_{1.8}O_4$ coatings on the surface of Crofer 22 H mesh, respectively. The commercial $CuMn_2O_4$ coating has thickness of approximately 5 μm and porosity of approximately 48% (estimated by ImageJ software on multiple SEM images). In contrast, the lab-developed $CuMn_{1.8}O_4$ coating is slightly thicker with thickness of approximately 10 μm, and it appears to be relatively denser with porosity of approximately 4%.

SEM images of top views of $CuMn_2O_4$ coating and $CuMn_{1.8}O_4$ coating are shown in Fig. 2c and d respectively. Again, compared with the commercial $CuMn_2O_4$ coating, the lab-developed $CuMn_{1.8}O_4$ coating is much denser with nearly no gap between the spinel grains. The average grain size of $CuMn_2O_4$ coating is approximately 0.52 μm, and that of $CuMn_{1.8}O_4$ coating is approximately 0.63 μm.

Fig. 2e shows the XRD patterns measured on the surface of these two coatings. Compared with $CuMn_2O_4$ coating, the diffraction peaks of $CuMn_{1.8}O_4$ are slightly to the right, indicating a slight smaller lattice parameter in the case of $CuMn_{1.8}O_4$ coating. By averaging the lattice constants calculated from (220) peak (at 2θ of ~30.3) and (311) peak (at 2θ of ~35.8), lattice constants for $CuMn_{1.8}O_4$ and $CuMn_2O_4$ are found to be 0.8314 nm and 0.8324 nm, respectively. The higher lattice constant of $CuMn_2O_4$ could be due to the fact that there are more Mn ions in the lattice. In both coatings, diffraction peaks of cubic spinel phases, Fe-Cr substrates, and slight amounts of Mn_3O_4 are observed.

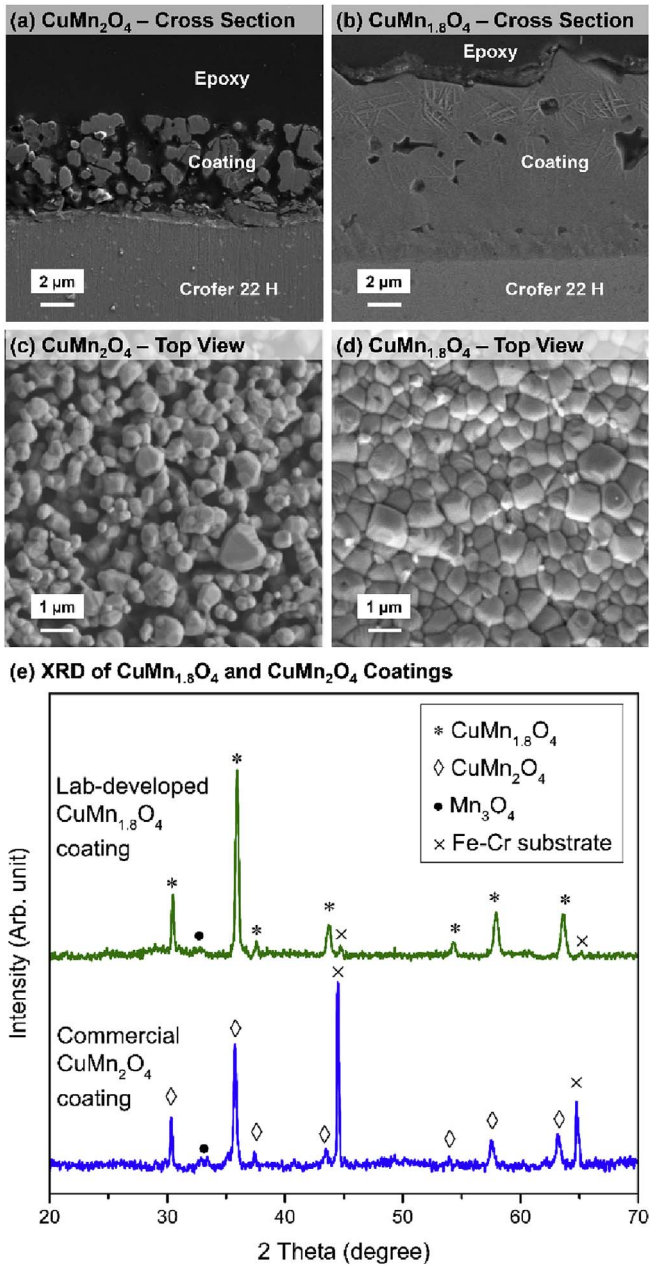

Fig. 2. SEM micrographs of the cross sections and the top views of coatings before on-cell testing: (a, c) commercial $CuMn_2O_4$ coating, and (b, d) lab-developed $CuMn_{1.8}O_4$ coating. (e) XRD results of $CuMn_2O_4$ and $CuMn_{1.8}O_4$ coatings before on-cell testing.

3.2. Cell test results

3.2.1. Cell performances under open-circuit condition

As mentioned in Section 2.3, cells were initially operated under open-circuit condition for 48 h. Fig. 3a and b show the impedance spectra measured of Cells 1, 2 and 3 measured at 0 h and after 48 h of open-circuit condition, respectively. In an impedance spectrum (represented by a Nyquist plot), the high-frequency intercept on the real axis corresponds to the area specific ohmic resistance (R_Ω) of the cell. The difference between high frequency intercept and low frequency intercept corresponds to the area specific electrode polarization resistance (R_p). The results of EIS measurements in the first 48 h can be described as follows:

a. The ohmic resistances (R_Ω) of the cells tested with uncoated (Cell 1), $CuMn_2O_4$ coated (Cell 2) and $CuMn_{1.8}O_4$ coated (Cell 3) interconnect meshes were 0.24, 0.20 and 0.18 Ω·cm^2, respectively, and during the 48 h of open-circuit condition the values did not change. Comparing the ohmic resistances between the cells, it is found that cells tested with spinel-coated meshes have lower R_Ω's and Cell 3 (tested with $CuMn_{1.8}O_4$ coated mesh) shows lowest R_Ω among the three cells.
b. At 0 h, the area specific polarization resistances (R_p) of Cells 1, 2 and 3 were 1.89, 1.85 and 1.74 Ω·cm^2, respectively (see Fig. 3a). The initial R_p's of these cells appeared to be relatively close, which is reasonable since the cells were fabricated under identical conditions.
c. At 48 h, the area specific polarization resistances (R_p) of Cells 1, 2 and 3 were 1.91, 1.55 and 1.22 Ω·cm^2, respectively (see Fig. 3b). Compared with their initial values measured at 0 h, R_p of Cell 1 (tested with uncoated interconnect) slightly increased by 1.1%, R_p of Cell 2 (tested with $CuMn_2O_4$ coated interconnect) decreased by 16.2%, and R_p of Cell 3 (tested with $CuMn_{1.8}O_4$ coated interconnect) decreased by 29.9%. The changes of R_p of these cells are also summarized in Fig. 3c. While the decrease of R_p for the cells tested with spinel-coated interconnects (Cells 2 and 3) can be ascribed to the cell break-in Refs. [13,23,49–52], the slight increase (instead of decrease) of R_p for cell tested with uncoated interconnect (Cell 1) clearly indicates that some Cr-poisoning through the chemical route occurred under open-circuit condition, which dominates over the improvement seen during the cell break-in.

The C-V curves and the corresponding power density curves of the cells measured at 0 h and at 48 h are displayed in Fig. 3d and e. At 0 h, the maximum power densities of Cells 1, 2 and 3 were 0.36 W/cm^2, 0.35 W/cm^2 and 0.40 W/cm^2, respectively. At 48 h, due to the cell break-in, the maximum power densities for the above-mentioned cells increased to 0.41 W/cm^2 (by ~14%), 0.51 W/cm^2 (by ~46%), and 0.61 W/cm^2 (by ~53%), respectively. In the case of Cell 1 (tested with uncoated meshes), the extents of increase in maximum power density due to cell break-in was significantly smaller than the cells that were tested with spinel-coated meshes, again indicating that the cell break-in of Cell 1 was counteracted by the Cr-related degradation under open-circuit condition.

Overall, the observations from C-V measurements and from EIS measurements agreed with each other, showing highest improvement of performance of Cell 3 (tested with $CuMn_{1.8}O_4$ coated mesh), moderate improvement of performance of Cell 2 (tested with $CuMn_2O_4$ coated mesh), and no/minimal improvement of performance of Cell 1 (tested with uncoated mesh).

3.2.2. Cell performances under galvanostatic condition

After 48 h of open-circuit condition, the cells were operated under galvanostatic condition at 0.5 A/cm^2. Fig. 4a shows the area specific polarization resistances (R_p) and area specific ohmic resistances (R_Ω) obtained from EIS measurements as functions of time for Cells 1, 2 and 3. The results of EIS measurements after t = 48 h can be described as follows:

a. In these three cells, no significant changes of area specific ohmic resistances (R_Ω) were observed. At the ends of the experiments, the area specific ohmic resistance of Cells 1, 2 and 3 were measured to be 0.19, 0.20, and 0.14 Ω·cm^2, respectively, which indicates that the lab-developed $CuMn_{1.8}O_4$ coating provided distinctly better electrical conductivity.
b. The area specific polarization resistances (R_p) of Cell 1 (tested with uncoated mesh) and Cell 2 (tested with $CuMn_2O_4$ coated mesh) were found to decrease at the beginning of the galvanostatic testing, and then they started to increase. The behavior that R_p decreases initially and then increases was also observed by some other authors [1,23,53–55], and can be ascribed to the activation effect (cell break-in) of cathodic current on cell performance. The increase in

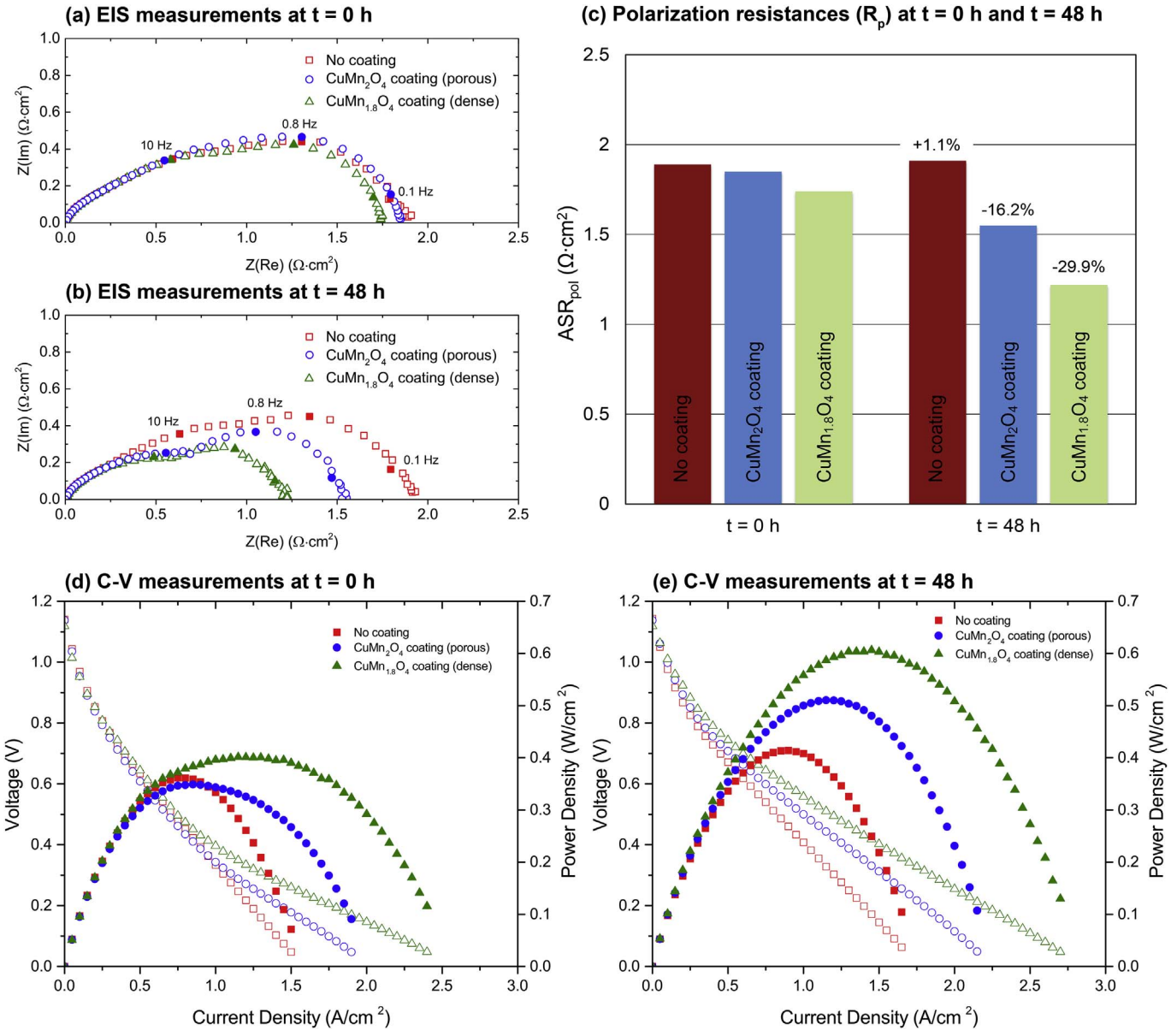

Fig. 3. (a, b) Impedance spectra of Cell 1 (with no coating on mesh), Cell 2 (with $CuMn_2O_4$ coated mesh) and Cell 3 (with $CuMn_{1.8}O_4$ coated mesh) measured under open-circuit condition at 800 °C in dry air at (a) t = 0 h, and (b) t = 48 h (the high frequency intercepts are normalized to zero for comparing the non-ohmic polarization resistances). (c) Comparison of polarization resistances (R_p) before and after 48 h of open-circuit conditions. (d, e) C-V curves and corresponding power density curves measured at 800 °C in dry air at (d) t = 0 h, and (e) t = 48 h.

the R_p values after the decrease for Cells 1 and 2 can be ascribed to the degradation caused by the Cr-poisoning effect. The rate of increase of the R_p value for Cell 2 is less than that of Cell 1 indicating the beneficial effect of the $CuMn_2O_4$ coating in decreasing the performance degradation due to Cr-poisoning.

c. In contrast, R_p of Cell 3 (tested with $CuMn_{1.8}O_4$ coated mesh) is relatively stable during galvanostatic testing. The relatively stable R_p of Cell 3 is due to the fact that the cell performance of Cell 3 has already improved during the first 48 h of cell break-in under open-circuit condition and there was no impact of Cr-poisoning. Overall, R_p of Cell 3 was the lowest, compared to that of Cells 1 and 2.

Fig. 4b shows the Nyquist plot of Cells 1, 2 and 3 measured before and after galvanostatic conditions. The activation effect of cathodic current on the cell performance in Cell 3 was much less compared to that in Cells 1 and 2 and agreeing with all the conclusions presented from Fig. 4a.

The cell performances were also characterized using C-V measurements. Fig. 5a shows the cell potentials at 0.5 A/cm^2 (obtained from C-V measurements) as a function of time for the cells tested with different interconnect meshes. The cell performances can be described as follows:

a. Cell 1 (with no coating): When there was no protective coating over the interconnect mesh, significant degradation of cell performance was observed under the galvanostatic condition (0.5 A/cm^2). The cell performance degradation was most rapid in the first 24 h and then the rate of degradation decreased. Overall, the cell potential at 0.5 A/cm^2 decreased from 0.67 V to 0.47 V (degraded by ~30%) during the 144 h of galvanostatic testing.

b. Cell 2 (with $CuMn_2O_4$ coated mesh): In the case of commercial $CuMn_2O_4$ spinel coating, cell performance increased slightly in the first 24 h of galvanostatic testing, and then stable for the next 144 h of galvanostatic testing (72 h–216 h in Fig. 5a). However, degradation was observed starting from 216 h (see Fig. 5a). In total,

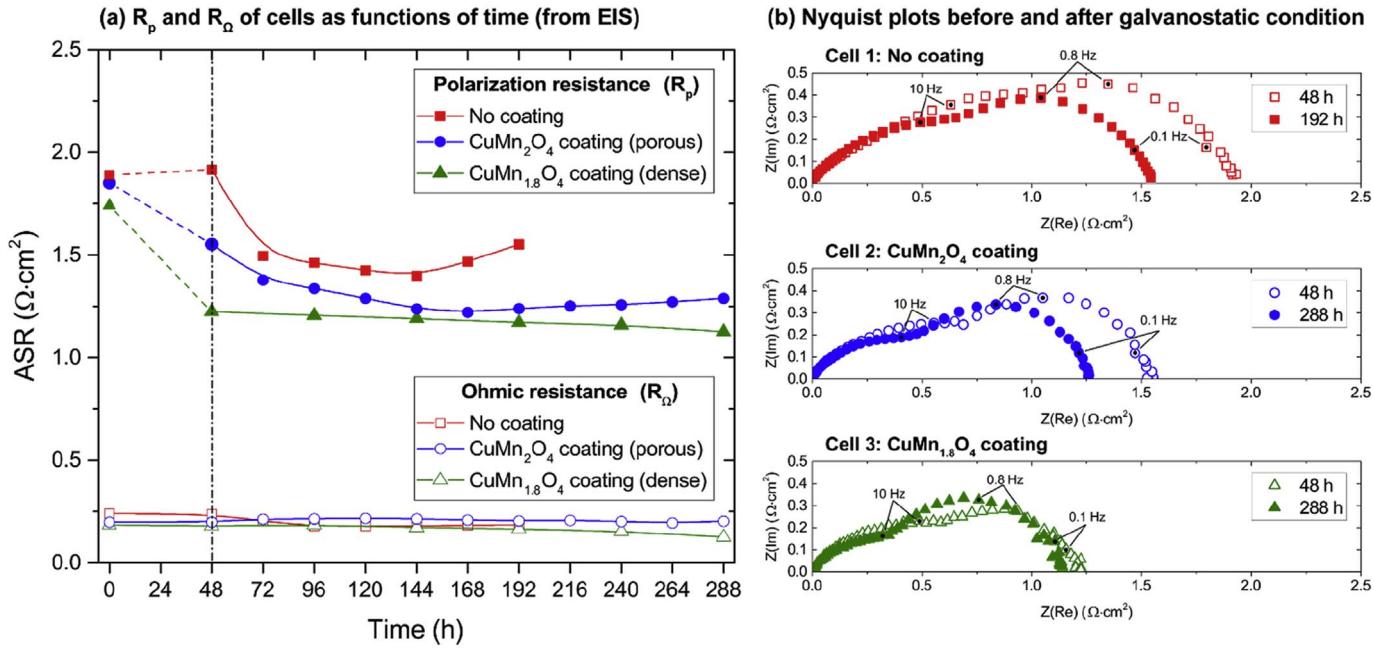

Fig. 4. (a) Area specific polarization resistances (R_p) and ohmic resistances (R_Ω) obtained from EIS measurements as functions of time for Cell 1 (with no coating on mesh), Cell 2 (with $CuMn_2O_4$ coated mesh) and Cell 3 (with $CuMn_{1.8}O_4$ coated mesh). (b) Nyquist plots of Cells 1, 2 and 3 obtained before and after galvanostatic condition (the high frequency intercepts are normalized to zero for comparing the non-ohmic polarization resistances).

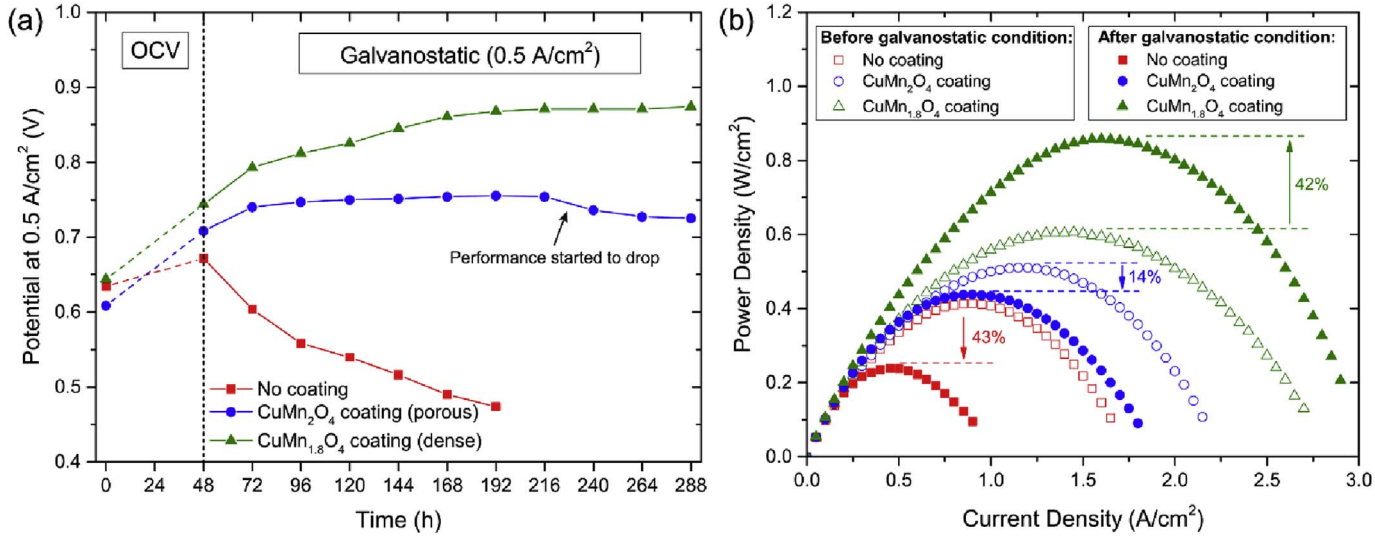

Fig. 5. (a) Cell potentials at 0.5 A/cm^2 as functions of time, with uncoated (Cell 1), $CuMn_2O_4$ coated (Cell 2) and $CuMn_{1.8}O_4$ coated (Cell 3) interconnect meshes as cathode current collectors. (b) Power density curves of the cells measured at t = 48 h and at the ends of the experiments (i.e. before and after the galvanostatic conditions).

the cell potential at 0.5 A/cm^2 increased from 0.71 V to 0.73 V (improved by ~3%) in the 240 h of galvanostatic condition.

c. Cell 3 (with $CuMn_{1.8}O_4$ coated mesh): In contrast, when lab-developed $CuMn_{1.8}O_4$ spinel coating was employed, no performance degradation was observed during the entire experiment. The cell potential at 0.5 A/cm^2 increased from 0.74 V to 0.87 V in 240 h of galvanostatic testing (improved by ~18%).

The power density curves before and after the galvanostatic condition of these cells are displayed in Fig. 5b. The maximum power density of Cell 1 (with no coating) decreased from 0.41 to 0.24 W/cm^2 (by ~43%), and that of Cell 2 (with $CuMn_2O_4$ coated mesh) decreased from 0.51 to 0.44 W/cm^2 (by ~14%). In contrast, the maximum power density of Cell 3 (with $CuMn_{1.8}O_4$ coated mesh) increased from 0.61 to 0.86 W/cm^2 (by ~42%).

Compared with open-circuit condition, galvanostatic condition (at 0.5 A/cm^2) significantly promoted the performance degradation when there was no protective coating over the interconnect mesh (Cell 1). This is considered to be due to the Cr-containing oxide scale over the uncoated Crofer 22 H mesh, which easily reacts with O_2 in the air, provides Cr vapor species that get electrochemically deposited in the cathode [13,23]. In contrast, when $CuMn_2O_4$ or $CuMn_{1.8}O_4$ spinel coating was applied over the Crofer 22 H mesh (Cell 2 or 3), slight or no degradation of cell performance was observed due to the suppression effects of the spinel coatings on the evaporation of Cr vapor species. However, comparing the two types of Cu-Mn spinel coatings, it was found that the performance of the lab-developed denser $CuMn_{1.8}O_4$ was distinct better, showing no observable degradation of cell performance (Cell 3).

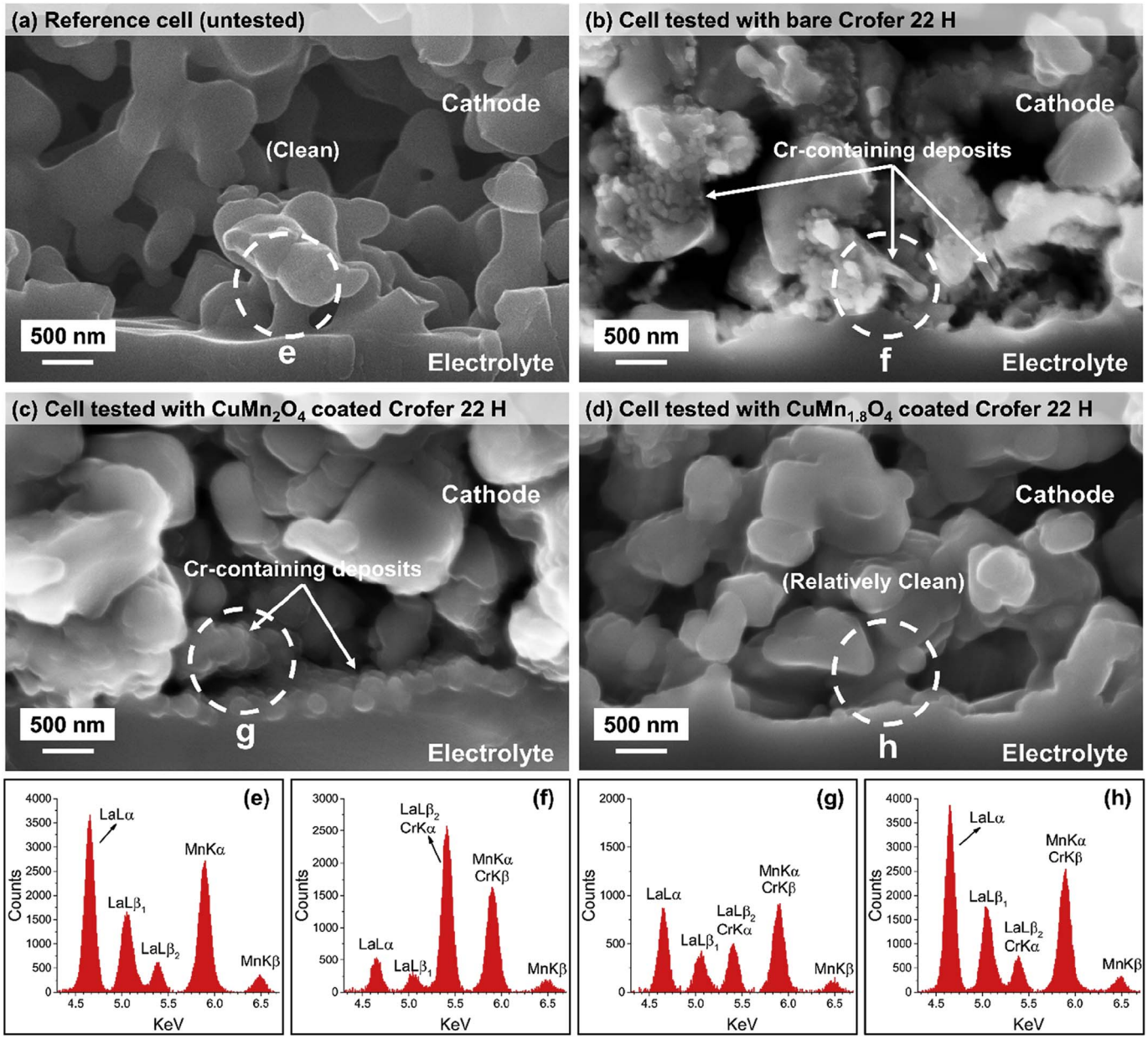

Fig. 6. SEM micrographs of cathode cross sections in: (a) untested reference cell, (b) Cell 1: tested with uncoated Crofer 22 H mesh, (c) Cell 2: tested with commercial $CuMn_2O_4$ coating, and (d) Cell 3: tested with lab-developed $CuMn_{1.8}O_4$ coating. (e-h) EDX spectra obtained from the dashed circles corresponding to Fig. 6a-d.

3.3. Microstructures of cell cathodes

Fig. 6a-d show the cross-sectional SEM micrographs near the cathode/electrolyte interfaces in (a) an untested reference cell, (b) Cell 1: tested with uncoated Crofer 22 H mesh, (c) Cell 2: tested with commercial $CuMn_2O_4$ coated Crofer 22 H mesh, and (d) Cell 3: tested with lab-developed $CuMn_{1.8}O_4$ coated Crofer 22 H mesh, respectively. Compared with the clean interface in the reference cell (Fig. 6a), the following differences are observed in the microstructures of Cells 1, 2 and 3:

a. In Cell 1 (with no coating), major amounts of Cr-containing deposits are observed near the cathode/electrolyte interface, and these deposits appear to extend several micrometers into the cathode (Fig. 6b).
b. In Cell 2 (with $CuMn_2O_4$ coated mesh), the Cr-containing deposits are mainly distributed at the cathode/electrolyte interface, where the amounts of deposits are much less than those in Cell 1 (Fig. 6c).
c. In contrast, the cathode/electrolyte interface in Cell 3 (with $CuMn_{1.8}O_4$ coated mesh) appears to be relatively clean with no observable Cr-containing deposits (Fig. 6d).

EDX analyses were performed to examine the elemental changes in the cathode cross sections of the cells after electrochemical testing. In the EDX analysis, overlap between $LaL\beta_2$ peak and CrKα peak in the X-ray spectrum are commonly observed in the La and Cr containing cathodes (such as LSM). In this study, the relative intensity ratio of the ($LaL\beta_2$ + CrKα)/LaLα was taken as an effective criterion of Cr deposition: a larger ($LaL\beta_2$ + CrKα)/LaLα intensity ratio indicates a higher amount of Cr deposits. The EDX spectra obtained from the dashed circular regions indicated in Fig. 6a-d are correspondingly shown in Fig. 6e-h. The intensity ratios of ($LaL\beta_2$ + CrKα)/LaLα were as follows: Cell 1 (4.78) > Cell 2 (0.61) > Cell 3 (0.20) > reference cell (0.17) (the dashed circular regions have diameters of 1 μm, which means that each EDX spectrum was collected from a point at the cathode/electrolyte interface). In the spectrum obtained in Cell 1

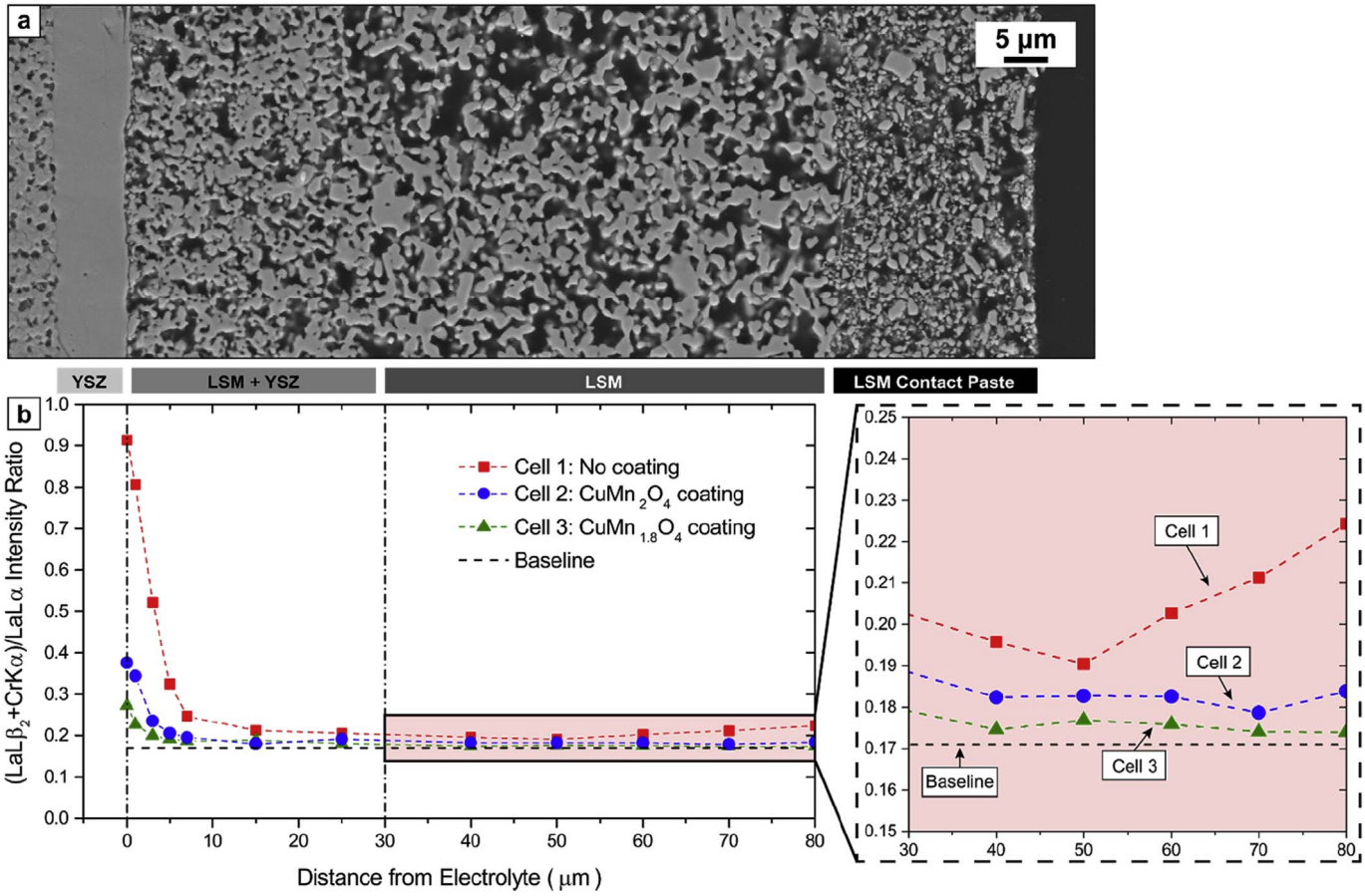

Fig. 7. (a) An example SEM image of cathode cross section after cell testing, showing three layers screen-printed/painted over the electrolyte: LSM + YSZ cathode active layer, LSM cathode current collector layer, and LSM contact layer. (b) ($LaL\beta_2$+CrKα)/LaLα intensity ratios as functions of distance away from the electrolyte in the cells tested with uncoated, $CuMn_2O_4$ coated and $CuMn_{1.8}O_4$ coated interconnect meshes (these average intensity ratios were obtained based on the EDX spectra collected from 2 μm × 16 μm rectangular areas).

(Fig. 6f), the intensities of Cr and Mn are distinctly higher, indicating that the deposits near the cathode/electrolyte interface are Cr,Mn-rich phases. These Cr and Mn containing deposits are likely $(Cr,Mn)_3O_4$ spinels, which were reported by many other researchers [18,21,56]. In the case of Cells 2 and 3 (Fig. 6g and h), only slightly higher intensities of Cr than the baseline value were detected. Due to the limited resolution of SEM/EDX, the exact compositions of Cr-containing deposits are difficult to determine, and higher resolution EDX analysis is needed.

To quantify and compare the amounts of Cr concentrations in the cathodes of the three tested cells, EDX spectra were collected from rectangular areas (2 μm in the direction of cathode bulk, 16 μm parallel to the electrolyte) at 0, 1, 3, 5, 7, 15, 25, 40, 50, 60, 70 and 80 μm away from the cathode/electrolyte interface, and the average intensity ratios of ($LaL\beta_2$ + CrKα)/LaLα were obtained. Fig. 7a shows an example SEM image of cathode cross section after cell testing, showing three layers screen-printed/painted over the YSZ electrolyte: LSM + YSZ cathode active layer (~30 μm), LSM cathode current collector layer (~50 μm), and LSM contact layer (~10 μm). Fig. 7b shows the ($LaL\beta_2$ + CrKα)/LaLα intensity ratios as a function of distance away from the cathode/electrolyte interfaces in the cell tested with uncoated, $CuMn_2O_4$ coated and $CuMn_{1.8}O_4$ coated interconnect meshes (the cathode thickness is correspondingly aligned with the SEM image shown in Fig. 7a). The Cr concentration profiles in the cells can be summarized as follows:

a. Cell 1: When cell was tested with uncoated Crofer 22 H mesh, a steep concentration gradient of Cr-containing deposits was observed near the cathode/electrolyte interface. The ($LaL\beta_2$ + CrKα)/LaLα intensity ratio at the cathode/electrolyte interface was measured to be 0.91, which indicates that large amounts of Cr-containing species were deposited close to the cathode/electrolyte interface.
b. Cell 2: When commercial $CuMn_2O_4$ coated Crofer 22 H mesh was employed, the concentration gradient near the cathode/electrolyte was more gradual. The ($LaL\beta_2$ + CrKα)/LaLα intensity ratio at cathode/electrolyte interface was measured to be 0.38, indicating smaller amount of Cr-containing deposits compared with that in the cell tested with uncoated mesh.
c. Cell 3: When the cell was tested with lab-coated dense $CuMn_{1.8}O_4$ coated Crofer 22 H mesh, the ($LaL\beta_2$ + CrKα)/LaLα intensity ratio near the cathode/electrolyte interface was only 0.27, indicating minor amount of Cr-containing deposits.

The ($LaL\beta_2$ + CrKα)/LaLα intensity ratios obtained in the cathode current collector layers (~30–80 μm away from electrolyte) are also shown in the zoomed-in plot in Fig. 7b (on the right). Interestingly it was found that a Cr concentration gradient relative to the surface of the cathode current collector layer (~50 - 80 μm away from electrolyte) developed in Cell 1. Since there is no protective coating on the surface of Crofer 22 H mesh used in Cell 1 testing, the higher intensity of Cr at the cathode surface compared with that in the bulk of LSM cathode current collector layer, suggests a solid-state diffusion pathway for Cr species in addition to the gas transport pathway. This solid-state diffusion pathway of Cr from interconnect to cathode was also reported and suggested by other researchers [57–59]. In contrast, when the interconnect mesh was coated with $CuMn_2O_4$ (Cell 2) or $CuMn_{1.8}O_4$ spinel (Cell 3), no intensity gradient of Cr was observed at cathode surface, indicating that the protective coating acted not only as a suppression layer for Cr vaporization, but also as a barrier layer for Cr solid-state diffusion.

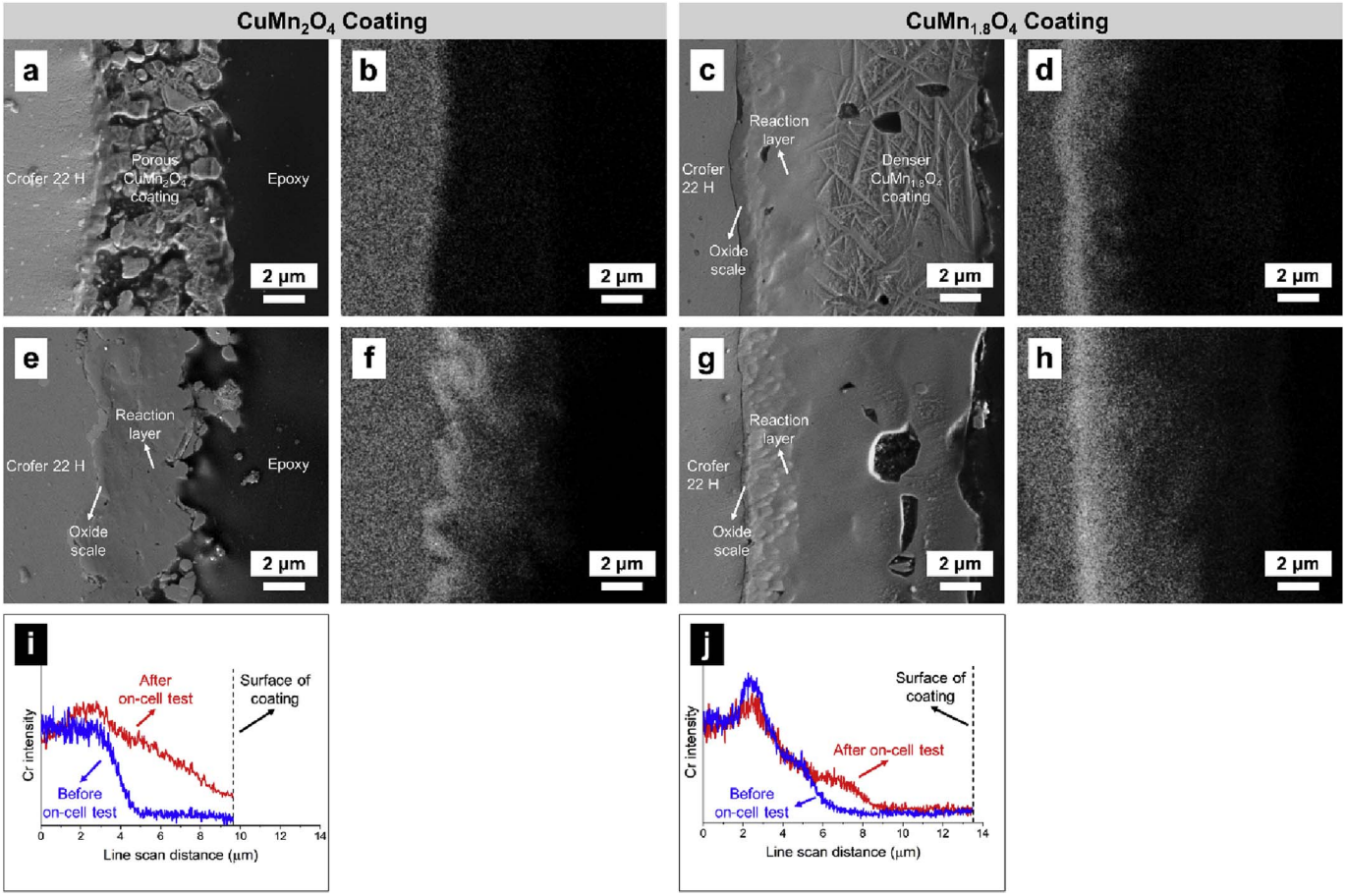

Fig. 8. SEM micrographs of $CuMn_2O_4$ coating and $CuMn_{1.8}O_4$ coating (a, c) before and (e, g) after 288 h of on-cell testing in air at 800 °C. (b, d, f, h) On the right of SEM images are EDX maps of Cr in the corresponding samples. (i, j) Cr intensity profile before and after 288 h of on-cell tests (in air at 800 °C) in the cross-sections of (i) porous commercial $CuMn_2O_4$ spinel coating, and (j) lab-developed dense $CuMn_{1.8}O_4$ spinel coating.

3.4. Characterizations of coatings after on-cell testing

Fig. 8a, e, c, and g show the cross-sectional SEM micrographs of the two types of coatings ($CuMn_2O_4$ spinel coating and $CuMn_{1.8}O_4$ spinel coating) on the Crofer 22 H mesh before and after the cell testing. The corresponding EDX mapping of Cr in the cross-sections of the coatings are shown in Fig. 8b, f, d, and h. Before cell testing, a Cr diffusion layer (between Cr-containing oxide scale and the coating) was found in the lab-developed $CuMn_{1.8}O_4$ coating (see Fig. 8d), which is not present for the commercial $CuMn_2O_4$ coating (see Fig. 8b). This is due to the fact that $CuMn_{1.8}O_4$ coating was annealed in air at 850 °C for 100 h, while $CuMn_2O_4$ coating was annealed for only 3 h. After the cell testing, both $CuMn_2O_4$ spinel coating and $CuMn_{1.8}O_4$ spinel coating were found to be well adhered to the interconnects, indicating good thermal compatibility between the coatings and the interconnect material. In the case of the porous $CuMn_2O_4$ spinel coating, the coating became dense after cell testing. The result of the EDX mapping shows that a reaction layer rich in Cr developed between $CuMn_2O_4$ coating and Crofer 22 H and the Cr begins to diffuse throughout the coating. In the case of lab-developed $CuMn_{1.8}O_4$ spinel coating, it was found that the diffusion of Cr from the reaction layer into the coating was limited. It is worth mentioning that the oxide scale in $CuMn_{1.8}O_4$ coating appears to be thinner after on-cell testing, compared with that before the cell testing (See Fig. 8c and g). The thickness of Cr_2O_3 layer depends on two competing factors: (a) oxidation of the substrates that forms new Cr_2O_3 and thus increases its thickness, and (b) consumption of this layer due to its reaction with the coating layer which decreases its thickness (forming a Cr-containing reaction layer). The thinner oxide scale indicates that the rate of consumption is larger than the rate of formation during the testing. While thinner oxide scale is beneficial to the cell performance because of the poor electrical conductivity of Cr_2O_3 (in comparison with that of Fe-Cr alloy and spinel coating), the effect of reaction layer is still unknown.

In order to examine and compare the Cr concentration profiles in these two types of Cu-Mn coatings before and after cell testing, EDX line scans were performed on the cross-sections of the spinel coatings. Fig. 8i and j show the Cr intensities in the porous commercial $CuMn_2O_4$ spinel coating and in the lab-developed dense $CuMn_{1.8}O_4$ spinel coating, before and after the 288 h on-cell testing. The EDX line scan results can be summarized as follows:

a. In the case of $CuMn_2O_4$ coating (Fig. 8i), a Cr concentration gradient developed in the coating cross section. The intensity of Cr on the surface of the coating after testing was found to be much higher than its initial value before testing, indicating Cr diffusion into the coating and reaching the surface.
b. In the case of $CuMn_{1.8}O_4$ coating (Fig. 8j), after the cell test, the Cr diffusion is limited within the dense inner layer of the coating, showing no distinct Cr intensity on the surface of the coating.

3.5. Summary of observations

In this study, based on the comparative experiments using uncoated, porous commercial $CuMn_2O_4$ spinel coated, and lab-developed denser $CuMn_{1.8}O_4$ spinel coated interconnect meshes, chromium poisoning phenomena are comprehensively investigated through cell electrochemical performance, cathode microstructures, and coating microstructures. The observations can be summarized and discussed as follows:

a. Cr-poisoning can occur under open-circuit condition through chemical pathway. Although chemical pathway of Cr-poisoning has been proposed by other researchers [15,20], it is shown in this study that the cell activation (or break-in) under open-circuit condition can be counteracted/restrained by the presence of Cr vapor species (shown in both C-V and EIS measurements). Therefore, when studying the Cr-related degradation of SOFC cathodes, care needs to be taken during the cell heat-up and equilibration processes, to account for the Cr environment that already exists before the cell testing begins.
b. Compared with open-circuit condition, galvanostatic condition at 0.5 A/cm^2 significantly promoted the performance degradation when cell was tested with uncoated interconnect (Cell 1). This is considered to be due to the Cr-containing oxide scale over the uncoated interconnect that easily reacts with O_2 in the air and provides large amounts of Cr vapor species which are electrochemically deposited in the cathode [13,23]. In contrast, when $CuMn_2O_4$ or $CuMn_{1.8}O_4$ spinel coating was applied over the Crofer 22 H mesh (Cells 2 and 3), slight or no degradation was observed due to the mitigation effects of the spinel coatings on the evaporation of Cr vapor species.
c. In addition to the gaseous transport of Cr species, surface diffusion of Cr through grain boundaries proposed by Tucker et al. is also possible [57,58]. A Cr intensity gradient relative to the surface of the cathode was observed in the cell tested with uncoated interconnect mesh (Cell 1), which was not the case for the cells tested with spinel-coated interconnect meshes (Cell 2 and 3). It is considered that the spinel coating acted not only as a suppression layer for Cr vaporization, but also as a barrier layer for direct contact between cathode materials and Cr-containing oxide scale over the interconnect, thereby preventing solid-state diffusion of Cr species.
d. Comparing the porous commercial $CuMn_2O_4$ spinel coating and lab-developed dense $CuMn_{1.8}O_4$ spinel coating, different observations in cell performance, cell microstructures and coating microstructures were found. In the case of commercial $CuMn_2O_4$ spinel coating, Cell 2 performance was stable at first and then started to show slight degradation. Considering the $CuMn_2O_4$ spinel coating is porous, it is likely that Cr vapor species started to evaporate through the pores of the coating layer at the beginning of the cell test. The stable performance at the beginning of the galvanostatic condition is considered to be due to the coexistence of the activation effect of cathodic current and the detrimental effect of Cr-poisoning. Starting at t = 216 h, Cell 2 performance degradation was observed (see Fig. 5a), and Cr intensity on the coating surface was no longer zero (see Fig. 8i). In contrast, when relatively denser $CuMn_{1.8}O_4$ spinel coating was applied on the interconnect, Cell 3 performance showed continuous improvement under galvanostatic condition which indicates that cell activation is effective and Cr-poisoning effect is negligible in this cell. Nearly no Cr-containing deposits was observed at the cathode/electrolyte interface of Cell 3, and the Cr diffusion was limited within the dense inner layer of the $CuMn_{1.8}O_4$ spinel coating. It is to be noted that higher stress and/or lower fracture toughness may be associated with a denser coating and therefore the effect of coating density on long term performance needs to be further investigated. It is also suggested that annealing and densification of the coating (under oxidizing atmosphere) should not be performed while cell testing, because Cr-poisoning may occur during annealing when the coating is not completely densified [40]. Overall, in order to minimize the effect of Cr-poisoning on cell performance during long-term operation, a dense and well-adherent protective coating on Fe-Cr alloy interconnect is necessary.

4. Conclusions

In this work, $CuMn_{1.8}O_4$ spinel coating was deposited on the surface of Crofer 22 H mesh by electrophoretic deposition (EPD) and successfully densified by a reduction and re-oxidation process. Anode-supported solid oxide fuel cells with LSM-based cathode were fabricated and electrochemically tested at 800 °C in the presence of Crofer 22 H mesh with no protective coating, that with porous commercial $CuMn_2O_4$ coating and the one with relatively denser $CuMn_{1.8}O_4$ coating.

Under open-circuit condition, the cell break-in was significant when the cell was tested with spinel-coated interconnect meshes but was negligible in the case of uncoated mesh. Cr-poisoning through the chemical route occurred under open-circuit conditions before the cell tests began. Under galvanostatic condition (0.5 A/cm^2), significant performance degradation was observed when no protective coating was applied over the interconnect mesh. In addition, a steep Cr concentration gradient was observed near the cathode/electrolyte interface, indicating that large amounts of Cr-containing species were electrochemically deposited during cell testing. In contrast, slight or no degradation in cell performance was observed when $CuMn_2O_4$ or $CuMn_{1.8}O_4$ coated interconnect mesh was used. Compared to the porous $CuMn_2O_4$ coating, the performance of the relative denser $CuMn_{1.8}O_4$ spinel coating was distinctly better, showing continuous improvement in cell performance and significantly less Cr deposition near the cathode/electrolyte interface after the test.

The cross-sections of the two types of Cu-Mn spinel coatings were also characterized and compared. It was found that the porous $CuMn_2O_4$ coating has poorer Cr gettering capacity, showing Cr diffusion out of the coating. In contrast, the Cr diffusion is limited within the dense inner layer of the $CuMn_{1.8}O_4$ coating, showing no distinct Cr intensity on the surface of the coating. This study shows that dense and long-term stable interconnect coatings are indispensable for mitigating the effects of Cr-poisoning, and the dense $CuMn_{1.8}O_4$ spinel coating shows great promise.

Acknowledgements

Financial support from U.S. Department of Energy, Office of Fossil Energy, through Award # FE0023325 is gratefully acknowledged.

References

[1] S. Badwal, R. Deller, K. Foger, Y. Ramprakash, J. Zhang, Interaction between chromia forming alloy interconnects and air electrode of solid oxide fuel cells, Solid State Ionics 99 (1997) 297–310.
[2] Y. Matsuzaki, I. Yasuda, Dependence of SOFC cathode degradation by chromium-containing alloy on compositions of electrodes and electrolytes, J. Electrochem. Soc. 148 (2001) A126–A131.
[3] W.Z. Zhu, S.C. Deevi, Development of interconnect materials for solid oxide fuel cells, Mater. Sci. Eng. A 348 (2003) 227–243.
[4] J.W. Fergus, Metallic interconnects for solid oxide fuel cells, Mater. Sci. Eng. A 397 (2005) 271–283.
[5] E.D. Wachsman, K.T. Lee, Lowering the temperature of solid oxide fuel cells, Science 334 (2011) 935–939.
[6] X. Chen, L. Zhang, E. Liu, S.P. Jiang, A fundamental study of chromium deposition and poisoning at $(La_{0.8}Sr_{0.2})_{0.95}(Mn_{1-x}Co_x)O_{3\pm\delta}$ $(0.0 \le x \le 1.0)$ cathodes of solid oxide fuel cells, Int. J. Hydrogen Energy 36 (2011) 805–821.
[7] N. Shaigan, W. Qu, D.G. Ivey, W. Chen, A review of recent progress in coatings, surface modifications and alloy developments for solid oxide fuel cell ferritic stainless steel interconnects, J. Power Sources 195 (2010) 1529–1542.
[8] J.C. Mah, A. Muchtar, M.R. Somalu, M.J. Ghazali, Metallic interconnects for solid oxide fuel cell: a review on protective coating and deposition techniques, Int. J. Hydrogen Energy 42 (2016) 9219–9229.
[9] S. Taniguchi, M. Kadowaki, H. Kawamura, T. Yasuo, Y. Akiyama, Y. Miyake, T. Saitoh, Degradation phenomena in the cathode of a solid oxide fuel cell with an alloy separator, J. Power Sources 55 (1995) 73–79.
[10] K. Hilpert, D. Das, M. Miller, D. Peck, R. Weiss, Chromium vapor species over solid oxide fuel cell interconnect materials and their potential for degradation processes, J. Electrochem. Soc. 143 (1996) 3642–3647.
[11] H. Kurokawa, C.P. Jacobson, L.C. DeJonghe, S.J. Visco, Chromium vaporization of bare and of coated iron–chromium alloys at 1073 K, Solid State Ionics 178 (2007) 287–296.
[12] J.W. Fergus, Effect of cathode and electrolyte transport properties on chromium poisoning in solid oxide fuel cells, Int. J. Hydrogen Energy 32 (2007) 3664–3671.
[13] R. Wang, M. Würth, U.B. Pal, S. Gopalan, S.N. Basu, Roles of humidity and cathodic

current in chromium poisoning of Sr-doped $LaMnO_3$-based cathodes in solid oxide fuel cells, J. Power Sources 360 (2017) 87–97.
[14] S.P. Jiang, J.P. Zhang, X.G. Zheng, A comparative investigation of chromium deposition at air electrodes of solid oxide fuel cells, J. Eur. Ceram. Soc. 22 (2002) 361–373.
[15] S.P. Jiang, X. Chen, Chromium deposition and poisoning of cathodes of solid oxide fuel cells–a review, Int. J. Hydrogen Energy 39 (2014) 505–531.
[16] T. Horita, Y. Xiong, H. Kishimoto, K. Yamaji, M.E. Brito, H. Yokokawa, Chromium poisoning and degradation at $(La,Sr)MnO_3$ and $(La,Sr)FeO_3$ cathodes for solid oxide fuel cells, J. Electrochem. Soc. 157 (2010) B614–B620.
[17] T. Horita, D.H. Cho, F. Wang, T. Shimonosono, H. Kishimoto, K. Yamaji, M.E. Brito, H. Yokokawa, Correlation between degradation of cathode performance and chromium concentration in $(La,Sr)MnO_3$ cathode, Solid State Ionics 225 (2012) 151–156.
[18] M. Krumpelt, T.A. Cruse, B.J. Ingram, J.L. Routbort, S. Wang, P.A. Salvador, G. Chen, The effect of chromium oxyhydroxide on solid oxide fuel cells, J. Electrochem. Soc. 157 (2010) B228–B233.
[19] L. Blum, L.B. de Haart, J. Malzbender, N.H. Menzler, J. Remmel, R. Steinberger-Wilckens, Recent results in Jülich solid oxide fuel cell technology development, J. Power Sources 241 (2013) 477–485.
[20] M. Kornely, A. Neumann, N.H. Menzler, A. Leonide, A. Weber, E. Ivers-Tiffée, Degradation of anode supported cell (ASC) performance by Cr-poisoning, J. Power Sources 196 (2011) 7203–7208.
[21] D. Röhrens, A. Neumann, A. Beez, I.C. Vinke, L.G.J. de Haart, N.H. Menzler, Formation of chromium containing impurities in $(La,Sr)MnO_3$ solid-oxide-fuel-cell cathodes under stack operating conditions and its effect on performance, Ceram. Int. 42 (2016) 9467–9474.
[22] R. Wang, M. Würth, B. Mo, U.B. Pal, S. Gopalan, S.N. Basu, Effect of humidity and cathodic current on chromium poisoning of Sr-doped $LaMnO_3$-based cathode in anode-supported solid oxide fuel cells, ECS Trans. 75 (2017) 61–67.
[23] R. Wang, U.B. Pal, S. Gopalan, S.N. Basu, Chromium poisoning effects on performance of $(La,Sr)MnO_3$-based cathode in anode-supported solid oxide fuel cells, J. Electrochem. Soc. 164 (2017) F740–F747.
[24] R. Wang, Z. Sun, Y. Lu, U.B. Pal, S.N. Basu, S. Gopalan, Chromium poisoning of cathodes in solid oxide fuel cells and its mitigation employing $CuMn_{1.8}O_4$ spinel coatings on interconnects, ECS Trans. 78 (2017) 1665–1674.
[25] J. Froitzheim, G.H. Meier, L. Niewolak, P.J. Ennis, H. Hattendorf, L. Singheiser, W.J. Quadakkers, Development of high strength ferritic steel for interconnect application in SOFCs, J. Power Sources 178 (2008) 163–173.
[26] B. Kuhn, C.A. Jimenez, L. Niewolak, T. Hüttel, T. Beck, H. Hattendorf, L. Singheiser, W.J. Quadakkers, Effect of Laves phase strengthening on the mechanical properties of high Cr ferritic steels for solid oxide fuel cell interconnect application, Mater. Sci. Eng. A 528 (2011) 5888–5899.
[27] A.W.B. Skilbred, R. Haugsrud, The effect of dual atmosphere conditions on the corrosion of Sandvik Sanergy HT, Int. J. Hydrogen Energy 37 (2012) 8095–8101.
[28] T. Horita, Y. Xiong, K. Yamaji, N. Sakai, H. Yokokawa, Evaluation of Fe-Cr alloys as interconnects for reduced operation temperature SOFCs, J. Electrochem. Soc. 150 (2003) A243–A248.
[29] Z. Yang, J.S. Hardy, M.S. Walker, G. Xia, S.P. Simner, J.W. Stevenson, Structure and conductivity of thermally grown scales on ferritic Fe-Cr-Mn steel for SOFC interconnect applications, J. Electrochem. Soc. 151 (2004) A1825–A1831.
[30] M. Stanislowski, E. Wessel, K. Hilpert, T. Markus, L. Singheiser, Chromium vaporization from high-temperature alloys I. Chromia-forming steels and the influence of outer oxide layers, J. Electrochem. Soc. 154 (2007) A295–A306.
[31] R. Sachitanand, M. Sattari, J.E. Svensson, J. Froitzheim, Evaluation of the oxidation and Cr evaporation properties of selected FeCr alloys used as SOFC interconnects, Int. J. Hydrogen Energy 38 (2013) 15328–15334.
[32] H. Falk-Windisch, J.E. Svensson, J. Froitzheim, The effect of temperature on chromium vaporization and oxide scale growth on interconnect steels for Solid Oxide Fuel Cells, J. Power Sources 287 (2015) 25–35.
[33] Z. Yang, G. Xia, S.P. Simner, J.W. Stevenson, Thermal growth and performance of manganese cobaltite spinel protection layers on ferritic stainless steel SOFC interconnects, J. Electrochem. Soc. 152 (2005) A1896–A1901.
[34] Z. Yang, G. Xia, J.W. Stevenson, $Mn_{1.5}Co_{1.5}O_4$ spinel protection layers on ferritic stainless steels for SOFC interconnect applications, Electrochem. Solid-State Lett. 8 (2005) A168–A170.
[35] Z. Yang, G.G. Xia, X.H. Li, J.W. Stevenson, $(Mn,Co)_3O_4$ spinel coatings on ferritic stainless steels for SOFC interconnect applications, Int. J. Hydrogen Energy 32 (2007) 3648–3654.
[36] C.C. Mardare, M. Spiegel, A. Savan, A. Ludwig, Thermally oxidized Mn-Co thin films as protective coatings for SOFC interconnects, J. Electrochem. Soc. 156 (2009) B1431–B1439.
[37] H. Zhang, Z. Zhan, X. Liu, Electrophoretic deposition of $(Mn,Co)_3O_4$ spinel coating for solid oxide fuel cell interconnects, J. Power Sources 196 (2011) 8041–8047.
[38] J. Wu, C.D. Johnson, R.S. Gemmen, X. Liu, The performance of solid oxide fuel cells with Mn-Co electroplated interconnect as cathode current collector, J. Power Sources 189 (2009) 1106–1113.
[39] S.I. Lee, J. Hong, H. Kim, J.W. Son, J.H. Lee, B.K. Kim, H.W. Lee, K.J. Yoon, Highly dense Mn-Co spinel coating for protection of metallic interconnect of solid oxide fuel cells, J. Electrochem. Soc. 161 (2014) F1389–F1394.
[40] B. Talic, H. Falk-Windisch, V. Venkatachalam, P.V. Hendriksen, K. Wiik, H.L. Lein, Effect of coating density on oxidation resistance and Cr vaporization from solid oxide fuel cell interconnects, J. Power Sources 354 (2017) 57–67.
[41] A. Petric, H. Ling, Electrical conductivity and thermal expansion of spinels at elevated temperatures, J. Am. Ceram. Soc. 90 (2007) 1515–1520.
[42] M.R. Bateni, P. Wei, X. Deng, A. Petric, Spinel coatings for UNS 430 stainless steel interconnects, Surf. Coat. Technol. 201 (2007) 4677–4684.
[43] W. Huang, S. Gopalan, U.B. Pal, S.N. Basu, Evaluation of electrophoretically deposited $CuMn_{1.8}O_4$ spinel coatings on Crofer 22 APU for solid oxide fuel cell interconnects, J. Electrochem. Soc. 155 (2008) B1161–B1167.
[44] N.S. Waluyo, B.K. Park, S.B. Lee, T.H. Lim, S.J. Park, R.H. Song, J.W. Lee, $(Mn,Cu)_3O_4$-based conductive coatings as effective barriers to high-temperature oxidation of metallic interconnects for solid oxide fuel cells, J. Solid State Electrochem 18 (2014) 445–452.
[45] M. Galbo, K.J. Yoon, U.B. Pal, S. Gopalan, S.N. Basu, Evaluating electrophoretically deposited Cu-Mn-O spinel coatings on stainless steel substrates used in solid oxide fuel cell interconnects, in: A. Jha, C. Wang, N.R. Neelameggham, D.P. Guillen, L. Li, C.K. Belt, R. Kirchain, J.S. Spangenberger, F. Johnson, A.J. Gomes, A. Pandey, P. Hosemann (Eds.), Energy Technology 2015: Carbon Dioxide Management and Other Technologies, Springer International Publishing, Switzerland, 2015, pp. 337–344.
[46] N. Hosseini, M.H. Abbasi, F. Karimzadeh, G.M. Choi, Development of $Cu_{1.3}Mn_{1.7}O_4$ spinel coating on ferritic stainless steel for solid oxide fuel cell interconnects, J. Power Sources 273 (2015) 1073–1083.
[47] Z. Sun, S. Gopalan, U.B. Pal, S.N. Basu, $Cu_{1.3}Mn_{1.7}O_4$ spinel coatings deposited by electrophoretic deposition on Crofer 22 APU substrates for solid oxide fuel cell applications, Surf. Coat. Technol. 323 (2017) 49–57.
[48] G. Di Domenicantonio, P. Briois, A. Billard, R. Ihringer, Redox anode supported cell performances tested with different cathode materials, ECS Trans. 57 (2013) 867–876.
[49] C. Sun, R. Hui, J. Roller, Cathode materials for solid oxide fuel cells: a review, J. Solid State Electrochem. 14 (2010) 1125–1144.
[50] S. McIntosh, S.B. Adler, J.M. Vohs, R.J. Gorte, Effect of polarization on and implications for characterization of LSM-YSZ composite cathodes, Electrochem. Solid-State Lett. 7 (2004) A111–A114.
[51] W. Wang, S.P. Jiang, A mechanistic study on the activation process of $(La, Sr)MnO_3$ electrodes of solid oxide fuel cells, Solid State Ionics 177 (2006) 1361–1369.
[52] Y. Yu, J. Liu, H.O. Finklea, H. Abernathy, P.R. Ohodnicki, T. Kalapos, G.A. Hackett, Chemical analysis of activation process of LSM thin film electrode, ECS Trans. 78 (2017) 701–708.
[53] Y. Matsuzaki, I. Yasuda, Electrochemical properties of a SOFC cathode in contact with a chromium-containing alloy separator, Solid State Ionics 132 (2000) 271–278.
[54] S.P. Jiang, J.P. Zhang, K. Foger, Deposition of chromium species at Sr-doped $LaMnO_3$ electrodes in solid oxide fuel cells II. Effect on O_2 reduction reaction, J. Electrochem. Soc. 147 (2000) 3195–3205.
[55] X. Chen, Y. Zhen, J. Li, S.P. Jiang, Chromium deposition and poisoning in dry and humidified air at $(La_{0.8}Sr_{0.2})_{0.9}MnO_{3+\delta}$ cathodes of solid oxide fuel cells, Int. J. Hydrogen Energy 35 (2010) 2477–2485.
[56] S. Wang, T. Cruse, M. Krumpelt, B. Ingram, P. Salvador, Microstructural degradation of $(La,Sr)MnO_3$/YSZ cathodes in solid oxide fuel cells with uncoated E-brite interconnects, J. Electrochem. Soc. 158 (2011) B152–B158.
[57] M.C. Tucker, H. Kurokawa, C.P. Jacobson, L.C. De Jonghe, S.J. Visco, A fundamental study of chromium deposition on solid oxide fuel cell cathode materials, J. Power Sources 160 (2006) 130–138.
[58] G.Y. Lau, M.C. Tucker, C.P. Jacobson, S.J. Visco, S.H. Gleixner, L.C. DeJonghe, Chromium transport by solid state diffusion on solid oxide fuel cell cathode, J. Power Sources 195 (2010) 7540–7547.
[59] B. Wei, K. Chen, L. Zhao, Z. Lü, S.P. Jiang, Chromium deposition and poisoning at $La_{0.6}Sr_{0.4}Co_{0.2}Fe_{0.8}O_{3-\delta}$ oxygen electrodes of solid oxide electrolysis cells, Phys. Chem. Chem. Phys. 17 (2015) 1601–1609.